Accepted version for *Applied & Environmental Microbiology* 2021
Volume 87 Issue 19 e00878-21

Functional Expression of Two Unusual Acidic Peroxygenases from *Candolleomyces aberdarensis* in Yeasts by Adopting Evolved Secretion Mutations

Patricia Gomez de Santos[1,2], Manh Dat Hoang[1,3], Jan Kiebist[4], Harald Kellner[5], René Ullrich[5], Katrin Scheibner[6], Martin Hofrichter[5], Christiane Liers[5], Miguel Alcalde[1*]

[1] Department of Biocatalysis, Institute of Catalysis, CSIC, 28049 Madrid, Spain.

[2] EvoEnzyme S.L., Parque Científico de Madrid, C/Faraday 7, Campus Cantoblanco 28049 Madrid, Spain.

[3] Institute of Biochemical Engineering, Technical University of Munich, Boltzmannstr. 15, 85748 Garching, Germany.

[4]JenaBios GmbH, Löbstedter Str. 80, 07749 Jena, Germany.

[5] Department of Bio- and Environmental Sciences, TU Dresden, International Institute Zittau, 02763 Zittau, Germany.

[6] Institute of Biotechnology, Brandenburg University of Technology Cottbus-Senftenberg, Universitätsplatz 1, 01968 Senftenberg, Germany.

*Corresponding Author: malcalde@icp.csic.es

ABSTRACT

Fungal unspecific peroxygenases (UPOs) are emergent biocatalysts that perform highly selective C-H oxyfunctionalizations of organic compounds, yet their heterologous production at high levels is required for their practical use in synthetic chemistry. Here, we achieved functional expression in yeast of two new unusual acidic peroxygenases from *Candolleomyces* (*Psathyrella*) *aberdarensis* (*Pab*UPO) and their production at large scale in bioreactor. Our strategy was based on adopting secretion mutations from *Agrocybe aegerita* UPO mutant −PaDa-I variant− designed by directed evolution for functional expression in yeast, which belongs to the same phylogenetic family as *Pab*UPOs –long-type UPOs− and that shares 65% sequence identity. After replacing the native signal peptides by the evolved leader sequence from PaDa-I, we constructed and screened site-directed recombination mutant libraries yielding two recombinant *Pab*UPOs with expression levels of 5.4 and 14.1 mg/L in *S. cerevisiae*. These variants were subsequently transferred to *P. pastoris* for overproduction in fed-batch bioreactor, boosting expression levels up to 290 mg/L with the highest volumetric activity achieved to date for a recombinant peroxygenase (60,000 U/L, with veratryl alcohol as substrate). With a broad pH activity profile, ranging from 2.0 to 9.0, these highly secreted, active and stable peroxygenases are promising tools for future engineering endeavors, as well as for their direct application in different industrial and environmental settings.

Keywords: Unspecific peroxygenase, heterologous functional expression, *Saccharomyces cerevisiae*, *Pichia pastoris*, directed evolution.

Running title: Evolved acidic peroxygenases expressed by yeast.

IMPORTANCE

In this work, we incorporated several secretion mutations from an evolved fungal peroxygenase to enhance the production of active and stable forms of two unusual acidic peroxygenases. The tandem-yeast expression system based on *S. cerevisiae* for directed evolution and *P. pastoris* for overproduction in a ~300 mg/L scale, is a versatile tool to generate UPO variants. By employing this approach, we foresee that acidic UPO variants will be more readily engineered in the near future and adapted to practical enzyme cascade reactions that can be performed over a broad pH range to oxyfunctionalize a variety of organic compounds.

INTRODUCTION

Fungal unspecific peroxygenases (UPOs, EC 1.11.2.1) are extracellular heme-thiolate enzymes that are of particular interest in the field of industrial and environmental biocatalysis (1). UPOs act as promiscuous mono(per)oxygenases, inserting oxygen into non-activated C-H bonds (peroxygenase activity) and thereby unlocking a palette of two-electron oxidation reactions that have a wide range of applications in organic synthesis. Accordingly, UPOs can drive the hydroxylation of aromatic and aliphatic alkanes, the epoxidation of alkenes, *O*- and *N*-dealkylations, *N*- and *S*-oxygenations, and halogenations (2). In addition to their peroxygenase activity, UPOs carry out one-electron oxidation of phenolics (peroxidase activity) and thus, they are considered as hybrid/chimeric enzymes that combine the mechanism of action of generic peroxidases with the oxygenation mechanism described for P450 monooxygenases through the peroxide shunt-pathway (3). Indeed, UPO oxyfunctionalization chemistry is supported simply by H_2O_2, which acts as both the final electron acceptor and the oxygen donor, representing an attractive and less complex alternative to the more intensely studied P450s. Unlike the latter, UPOs are soluble extracellular enzymes that neither need expensive redox cofactors nor auxiliary flavoproteins, and they do not undergo O_2 uncoupling. For these reasons, UPOs are generating enormous interest in applied biocatalysis (4).

However, to establish UPOs as practical biocatalysts in the pharma, chemical and environmental sectors, it is paramount to develop robust heterologous expression platforms that guarantee their recombinant production and engineering by directed evolution (5). With more than 4,000 putative UPO sequences deposited in genomic databases, peroxygenases have been phylogenetically sorted into two families: Family I, short-type UPOs that typically form homodimers of ~26 kDa monomers and that carry a His residue as a charge stabilizer; and Family II, long-type UPOs, that are ~44 kDa monomeric enzymes with an Arg residue

as a charge stabilizer (3). Their different geometry in the heme channel along with the abovementioned characteristics, are responsible for different substrate profile and product selectivity among both UPO´s families.

Despite their ubiquitous abundance in the fungal kingdom, UPOs are difficult to express in heterologous organisms, with only limited success in yeasts, filamentous fungi and bacteria to date (6). In yeast, the best secreted peroxygenase is the long-type UPO from *Agrocybe aegerita* (syn. *Cyclocybe aegerita* − *Aae*UPO), with production levels of over 200 mg/L in a bioreactor. This UPO was engineered for expression in *Saccharomyces cerevisiae* and *Pichia pastoris* by directed evolution (7, 8) and the evolved *Aae*UPO mutant obtained (referred to as the PaDa-I variant) currently serves as a model expression system for many peroxygenase-based biocatalysis studies, along with tailored mutants for different applications (6, 8–16). Along similar lines, the long-type UPO from *Coprinopsis cinerea* (r*Cci*UPO) has been produced recombinantly in *Aspergillus oryzae* by Novozymes A/S (Bargsvaerd, Denmark) and it has also been widely studied, although the details of this expression system are not freely available (17). More recently, 9 short-type UPOs were added to this pool by applying a modular secretion system based on Golden Gate cloning in yeast together with 5 long-type UPO chimeras based on the PaDa-I mutant as main secretion scaffold (18–20). In addition, three more short-type UPO proteins were expressed in *Escherichia coli*, although the weak protein production seems to preclude their engineering by directed evolution (21–23).

Thus, at present only two long-type UPOs have been heterologously produced at reasonable titers in robust expression systems (the PaDa-I variant in yeast and *rCci*UPO in *A. oryzae*), which is why scientists are mining for more UPOs with new biochemical attributes that can be recombinantly expressed to open up new industrial possibilities and research opportunities. In this regard, all the UPOs hitherto reported display a pH profile for oxygen

transfer reactions close to neutral (pH 5.0 to 7.0), along with poor stability under acidic conditions (pH 2.0 to 3.0) (2, 3). This narrow pH window may limit their applications should they have to be combined with other enzymes in cascade reactions or used under more drastic conditions. Two years ago, two new long-type UPO genes from *Candolleomyces (Psathyrella) aberdarensis* (*Pab*UPO-I and *Pab*UPO-II), an East African ink-cap (24, 25), were identified and characterized. These peroxygenases have singular biochemical properties relative to previously described UPOs in terms of their pH activity and stability profiles, showing an unusual broad pH range for peroxygenase activity (from pH 2.0 to 9.0) and strong stability at alkaline or acidic pHs (depending on the isoform). These physicochemical properties of the *Pab*UPOs pinpoint specific adaptations of the native fungi to grow in the voluble fungal microenvironment that could be harnessed for different oxyfunctionalization reactions at acidic/basic pH (3, 26).

In the current study we describe the heterologous functional expression in two yeast species of these two new long-type *Pab*UPO genes. By replacing their original signal peptides, and constructing and screening site-directed recombination mutant libraries, the most beneficial secretion mutations from the PaDa-I variant were incorporated into *Pab*UPOs for their successful expression in *S. cerevisiae*. The best secretion clones were further transferred to *P. pastoris* for overproduction in a bioreactor and characterized biochemically. While the exclusive pH activity profiles of native *Pab*UPOs were conserved in the recombinant variants, production was boosted to approx. 300 mg/L, paving the way for the future industrial use of these unusual acidic peroxygenases.

RESULTS

Adopting mutations from the evolved PaDa-I variant

*Aae*UPO was engineered by directed evolution for heterologous functional expression and to the best of our knowledge, it is the strongest recombinant UPO expression reported

to date in yeast (7, 8). The wild type *Aae*UPO gene encodes a 328 amino acid mature protein preceded by a 43 amino acid signal peptide. We previously applied directed evolution to the signal peptide through focused mutagenesis, and to the mature *Aae*UPO protein by DNA shuffling and random mutation, through which we generated a final secretion mutant, PaDa-I, with improved expression by *S. cerevisiae* (8 mg/L) and by *P. pastoris* in a bioreactor (217 mg/L) (7, 8). The PaDa-I variant carries mutations F12Y-A14V-R15G-A21D-V57A-L67F-V75I-I248V-F311L (mutations in the signal peptide underlined) that induced a total activity improvement (TAI: the joint increase of specific activity and secretion) 3,250-fold that of the wild type *Aae*UPO. Since *Pab*UPOs share ~64-66% protein sequence identity with the PaDa-I mutant (**Supplementary Table S1**), we reasoned that some of the key elements that boosted heterologous *Aae*UPO expression could enhance *Pab*UPO secretion by yeast.

The *Pab*UPO-I and *Pab*UPO-II genes encode mature proteins of 333 and 348 amino acids, plus a 45 and 38 amino acid signal peptide respectively (26) (**Supplementary Fig. S1**). As such, we first prepared four expression constructs of *Pab*UPOs that were benchmarked for heterologous production by *S. cerevisiae*: *Nt*-PI and *Nt*-PII which correspond to *Pab*UPO-I and *Pab*UPO-II with their native signal peptides (*Nt*); and their counterparts *Ev*-PI and *Ev*-PII in which the corresponding *Nt* was replaced by the evolved signal peptide (*Ev*) from the PaDa-I mutant (previously seen to improve native *Aae*UPO functional expression 27-fold) (7). Despite the weak sequence identity between the *Nt* *Pab*UPO signal peptides and the *Ev* peptide from PaDa-I (12.5 and 41% for *Pab*UPO-I and *Pab*UPO-II, respectively, **Supplementary Fig. S2**), replacing the native signal peptides with the evolved leader sequence from PaDa-I had no deleterious effects but rather, it significantly enhanced secretion. Flask production of the different constructs indicated that the *Ev* peptide enhanced expression from 10 U/L of *Nt*-PI to 33 U/L for *Ev*-PI, and from 300 U/L of *Nt*-PII to 542 U/L of *Ev*-PII when 2,6-dimethoxyphenol (DMP) was used as a

substrate. Thus, replacing the *Nt Pab*UPO signal peptides with the *Ev* peptides from PaDa-I improved secretion by 3.3- and 1.8-fold, with production levels in flask of 2.1 and 5.4 mg/L for *Ev*-PI and *Ev*-PII, respectively.

It is worth noting that the native, non-evolved, *Aae*UPO is hardly secreted in *S. cerevisiae* (0.007 mg/L) and thus, the expression of *Pab*UPOs with the *Nt* signal peptides suggested that some of the mutations that improved the secretion and activity of PaDa-I might already be present in *Pab*UPOs. Hence, we mapped these substitutions by aligning the *Pab*UPO-I, *Pab*UPO-II and PaDa-I protein sequences (**Fig. 1**), identifying several matches in the *Pab*UPO sequences to the five mutations acquired by directed evolution in the mature PaDa-I variant (V57A-L67F-V75I-I248V-F311L). In particular there were three coincidences (Ala57, Phe67 and Ile75) in *Pab*UPO-II, whereas only Phe67 was present in *Pab*UPO-I. Moreover, Val248 was represented by a similar Leu residue in *Pab*UPO-II but by an Ala in *Pab*UPO-I. In PaDa-I, Phe311 was mutated to Leu, and at this position there was a Phe or a Trp in *Pab*UPO-I and *Pab*UPO-II, respectively (**Fig. 2**). Taken together, we reasoned that the weaker expression of *Pab*UPO-I in *S. cerevisiae* compared to that of *Pab*UPO-II could be related to the fewer secretion mutations, coinciding with those in PaDa-I. Consequently, we introduced the Ala57, Ile75 and Val/Leu248 substitutions into *Pab*UPO-I (replacing the original Ser61, Leu79 and Ala252 in the *Pab*UPO-I sequence) by *in-vivo* site-directed recombination (SDR). The F311L mutation from PaDa-I was not included in these experiments because this position is critical to regulate the trafficking of substrates to the heme, as recently observed in the crystal structure of the PaDa-I mutant through soaking experiments (27). SDR is a mutant library creation method based on the recombination machinery of *S. cerevisiae* that allows potential beneficial mutations, together with their reversions, to be rapidly recombined in a direct manner, allowing to identify the optimal combination of substitutions upon screening (28). After two rounds of SDR combined with

site-directed mutagenesis (**Fig. 3**), we identified a *Pab*UPO-I triple mutant S61A-L79I-A252L (named here Grogu) with expression levels boosted from 2.1 to 14 mg/L.

Bioreactor production of recombinant *Pab*UPOs in *P. pastoris* and their biochemical characterization

The expression of Grogu and *Pab*UPO-II in *S. cerevisiae* can aid future directed evolution campaigns, while the industrial production of these variants could be carried out in the methylotrophic yeast *P. pastoris* (*Komagataella phaffii*) given the high cell titers that can be achieved in this yeast together with the regulation by strong promoters. Accordingly, the production of the Grogu mutant and *Pab*UPO-II (both preceded by the *Ev* signal peptide) by *P. pastoris* was evaluated in 5-L fed-batch bioreactor (1.7 L culture volume). The strongest secreted and most stable multicopy variants were selected, and fermented following our previously described protocols (8), producing 240 mg/L Grogu and 290 mg/L *Pab*UPO-II. While these expression levels are both remarkable, the production of recombinant *Pab*UPO-II is particularly outstanding, since – to the best of our knowledge – it constitutes the highest volumetric activity of a peroxygenase (60,000 U/L measured with veratryl alcohol) described to date. The differences in expression of Grogu and *Pab*UPO-II between *S. cerevisiae* and *P. pastoris* (*i.e.* the heterologous expression in *S. cerevisiae* was in the order Grogu>*Pab*UPO-II whereas in *P. pastoris* was *Pab*UPOII>Grogu) may be related to the selection of the variants from the strain screening, with different copy numbers integrated into the *P. pastoris* genome.

Both the Grogu mutant and *Pab*UPO-II from *P. pastoris* were purified to homogeneity (Reinheitszahl value [Rz] [A_{418}/A_{280}]~2) and characterized biochemically (**Table 1, Supplementary Fig. S3)**. The molecular masses of Grogu and *Pab*UPO-II estimated by the average molecular mass measured by matrix-assisted laser desorption ionization–time of flight mass spectrometry (MALDI-TOF) were 42,491 and 41,247 Da respectively, with a ~9-

14% contribution of glycosylation deduced from their deglycosylated size (**Table 1**, **Supplementary Fig. S3, S4, S5)**. Kinetic thermostability was determined by measuring the T_{50} (the temperature at which the enzyme retained 50% of its activity after a 10 min incubation); obtaining T_{50} values of 56 ºC for Grogu and 61 ºC for recombinant *Pab*UPO-II (**Fig. 4A**), both in the range of that reported for the PaDa-I mutant (55 ºC) (7, 8). In terms of the pH profiles for peroxygenase activity, both recombinant UPOs produced similar curves to the wild type *Pab*UPOs from the original fungus. The Grogu mutant retained roughly 60% relative activity in the pH range from 3.0 to 9.0, measured with veratryl alcohol, and more than 80% activity at pH 4.0 to 8.0 with an optimum value at pH 6.0. By contrast, optimal recombinant *Pab*UPO-II activity was evident at pH 5.0, retaining over 40% of its relative activity in the pH range from 4.0 to 7.0 (**Fig. 4B**). In terms of their pH stability, recombinant *Pab*UPO-II was stable at alkaline pH but like the wild type *Pab*UPO-II, it rapidly lost activity at acidic pHs (3, 26). By contrast, the Grogu mutant was fairly stable at both alkaline and acidic pHs (**Figs 4C, D**). With a sequence identity of 65% between Grogu mutant and *Pab*UPO-II, the differences in pH activity/stability profiles and in kinetic thermostability are likely to be produced in the regions of the protein with lower similarity, such as the N-terminus that differs significantly in the two variants. Such regions could be of interest as targets for future protein engineering studies (**Fig. 1**).

Kinetic constants were measured with prototypical peroxygenase substrates (veratryl alcohol, benzyl alcohol, 5-nitro-1,3-benzodioxole −NBD−) as well as with classic peroxidase substrates (2,2´-azino-bis(3-ethylbenzothiazoline-6-sulfonic acid) −ABTS− and DMP) (**Table 2**). The values with ABTS were close to each other and to those of the wild type enzymes, whereas the catalytic efficiency with DMP of recombinant *Pab*UPO-II was increased 3-fold relative to the Grogu mutant, following the same tendency as wild type *Pab*UPOs (3, 26). The catalytic efficiencies with veratryl alcohol were also quite similar, with

Grogu showing numbers similar to those of the wild type *Pab*UPO-I, while the K_m for recombinant *Pab*UPO-II increased 3-fold. With the *O*-dealkylation substrate NBD, both Grogu and recombinant *Pab*UPO-II shared virtually the same values, whereas *Pab*UPO-II had a higher K_m with benzyl alcohol. H_2O_2 catalytic parameters were measured with veratryl alcohol as a reducing substrate, with a higher K_m for recombinant *Pab*UPO-II but a similar k_{cat}/K_m for both enzymes, specifically due to a 3.4-fold increase in the k_{cat} of recombinant *Pab*UPO-II with respect to Grogu.

DISCUSSION

Unspecific peroxygenases (UPOs) and in particular long-type UPOs, are difficult to express in heterologous hosts. Indeed, after more than 15 years of research, only two successful examples of recombinant long-type UPOs with high production levels have been reported so far, the evolved PaDa-I mutant from *Aae*UPO and r*Cci*UPO, making these attractive blueprints for engineering and industrial applications. By contrast, several short-type UPOs have been produced heterologously (from *Marasmius rotula*, *Humicola insolens*, *Chaetomium globosum*, *Thielavia terrestris*, *Myceliophthora thermophila*, *Myceliophthora fergusii*, *Myceliophthora hinnulea*, *Collariela virescens* and *Daldinia caldariorum*) (19, 29). In view of their higher structural complexity, it is somewhat paradoxical to see more recombinant short UPOs than long UPOs, particularly given their general dimeric nature and the intermonomer disulfide bridge that may demand even more complex posttranslational modifications than their long UPO counterparts (with the exceptions of *M. fergussi*, *M. hinnulea* and *T. terrestris* UPOs which lack the C-terminal Cys residue needed for the disulfide bridge and hence the dimeric form). While it remains unclear why the expression of long-type UPOs is so elusive, it may be related to the characteristic geometry of the heme cavity or the need for an internal disulfide bridge at the C-terminal for correct folding. Here, we overcame the shortcomings in expressing long-type UPOs by adopting the mutational

backbone of the evolved PaDa-I secretion mutant. Thereby we achieved the highest volumetric activity level (for *Pab*UPO-II with 60,000 U/L using veratryl alcohol as substrate to be oxyfunctionalized) reported so far for both recombinant and wild-type UPOs. A comparable volume activity (up to 41,000 U/L) has only been demonstrated for the short-type wild-type UPO secreted by the basidiomycetous fungus *Marasmius rotula* (30).

Wild type *Pab*UPO-I and *Pab*UPO-II are expressed by yeast, which is of note for long-type UPOs, and this expression was further increased by switching their signal peptide for the evolved signal sequence of PaDa-I. Hence, some of the secretion related mutations introduced into the mature PaDa-I protein may be incorporated into *Pab*UPOs to enhance their expression. Of the five mutations in PaDa-I, *PabU*PO-II carried three exact matches and one synonymous change, whereas *Pab*UPO-I carried only one exact match. By constructing and screening SDR mutant libraries, we found an optimal combination of secretion mutations that improved *Pab*UPO-I yielding the Grogu variant, surpassing the expression of PaDa-I in *S. cerevisiae*. Of the five PaDa-I secretion mutations, V57A and L67F are overrepresented in long-type UPOs. Unlike Ile248, the original Val75 and in particular the Phe311 change are also predominant (**Fig. 5**). Given that recombinant *Pab*UPO-II, Grogu and PaDa-I variants share a similar secretion backbone, we hypothesize that UPO expression in the original fungus was a function of its physiological needs, and it may have been regulated in the course of evolution by removing (in the case of *Aae*UPO) or partially conserving (*Pab*UPOs) key residues for expression. The use of paleoenzymology by ancestral sequence reconstruction and resurrection is providing a new twist in enzyme engineering while it is also an invaluable strategy to mine the timeline of evolution (31, 32). By applying such methods, we have recently inferred several ancestral nodes from long-type UPOs that may help us to understand the natural role played by the secretion mutations

of PaDa-I and *Pab*UPOs counterparts as well as the evolutionary trajectory within this enzyme family (unpublished material).

At a structural level, we found that the heme environment of the *Pab*UPOs has a characteristic PCP motif (Pro39/51-Cys40/52-Pro41/53 in Grogu/*Pab*UPO-II) that places the thiolate (Cys-SH) of the proximal ligand (5^{th}) Cys towards the heme iron (**Fig. 6**). This conserved feature, together with the acid-base pair typical of long-type UPOs that is formed by the glutamic acid residue and an arginine (Glu199-Arg193/Glu212-Arg205 in Grogu/*Pab*UPO-II), is mainly responsible for the peroxide shunt pathway mechanism. The heme access channel is lined by aromatic amino acids, as occurs in PaDa-I, yet with some interesting differences. At the entrance of the heme channel, the pair of protruding Phe residues that permit the substrate to access the active site in PaDa-I are present in Grogu, whereas they are replaced by two aliphatic amino acids in *Pab*UPO-II (Val92-Ile207). Moreover, the aromatic triad formed by Phe69, Phe121 and Phe199 in PaDa-I, involved in orienting the substrate for catalysis (27, 33), is conserved in *Pab*UPO-II (Phe85, Phe137 and Phe215). However, the first of these residues is substituted by methionine in Grogu (Met73, Phe125 and Phe203), as also occurs in r*Cci*UPO (17).

In summary, our models seem to indicate that both the *Pab*UPOs are similar to the PaDa-I in terms of dimensions and in the amino acid composition of the heme channel, yet some important changes in this region may drive different substrate preferences and selectivity, which could favor their future engineering for specific applications.

CONCLUSIONS

Since the discovery of *Aae*UPO in 2004 (34), several other fungal peroxygenases have been described but only a few have been produced in heterologous hosts. The PaDa-I mutant is one of these, the product of five rounds of directed evolution to improve secretion by yeast, and it was used here as a template to improve the expression of two new long-

type UPOs. Taking lessons from our previous evolutionary campaigns, we expressed two unusual acidic *Pab*UPOs at very high levels in yeast. In particular, we harnessed the evolved signal peptide from PaDa-I, together with secretion mutations, to produce these *Pab*UPOs in a bioreactor with the highest volume activity reported so far. These UPOs are active and stable over a broad pH range. Since long-type UPOs seem to be more reluctant to heterologous functional expression than their short-type counterparts (with only 2 long-type UPOs and 9 short-type UPOs expressed in recombinant forms (7, 8, 18, 19, 21-23)), the strategy of adopting mutations from evolved secretion mutants may notably reduce the experimental effort required, and allow us to consider new engineering workflows to achieve functional heterologous expression of other long-type UPOs in a quick and simple manner in the future.

MATERIAL AND METHODS

Strains and chemicals

The *P. pastoris* expression vector (pPICZ-B), the *P. pastoris* strain X-33 and the antibiotic zeocin were purchased from Invitrogen (USA). The *Escherichia coli* strain XL2-Blue competent cells were obtained from Agilent Technologies (USA). Restriction endonucleases *Eco*RI, *Xba*I, *Pme*I, *Bam*HI and *Xho*I, the DNA Ligation Kit, the Antarctic phosphatase and the PNGase F were purchased from New England Biolabs (USA). iProof High-Fidelity DNA Polymerase was purchased from Bio-Rad (USA). Oligonucleotide primers and UPO genes were acquired from Integrated DNA Technologies (USA). NucleoSpin plasmid kit and NucleoSpin Gel and PCR Clean-up kit were purchased from Macherey Nagel (Germany). ABTS (2,2′-azino-bis(3-ethylbenzothiazoline-6-sulfonicacid)) was purchased to Panreac AppliChem (Germany), DMP (2,6-dimethoxyphenol) and NBD (5-nitro-1,3-benzodioxole) to TCI Europe (Switzerland) and veratryl alcohol, benzyl alcohol and H_2O_2

were purchased from Merck Life Science (USA). All chemicals and media components were of the highest purity available

Cloning of *Pab*UPOs in *S. cerevisiae*

The genes encoding for *Pab*UPO-I (c271g7491) and *Pab*UPO-II (c327g8238) from *Candolleomyces* (*Psathyrella*) *aberdarensis* (Mycobank no.: MB 827350, Genbank accession no.: MH880928) (24, 25) were ordered with codon optimization for *S. cerevisiae*. The synthetized genes (*Nt*-PI, *Nt*-PII, *Ev*-PI, *Ev*-PII containing overhangs to promote homologous recombination) were cloned under the control of the GAL1 promoter of the pJRoC30 expression shuttle vector, using *Bam*HI and *Xho*I restriction enzymes. The linearized vector was loaded onto a preparative agarose gel and purified with the NucleoSpin Gel and PCR Clean-up kit. The corresponding gene (200 ng each) was mixed with the linearized plasmid (100 ng) and transformed into *S. cerevisiae* for *in vivo* gene reassembly and cloning by IVOE (35).

Site-directed recombination (SDR) and site-directed mutagenesis

PCR reactions for site-directed recombination (SDR) were carried out according to supplementary **Fig. S6**. The primers used were RMLN (5'-cctctatactttaacgtcaagg-3'), S/A61 R (5'- ctcctgaacagcttcaattatctgagmcggtgtggccacacc-3'), S/A61-L/I79 F (5'-ggtgtggccacaccgkctcagataattgaagctgttcaggagggtttcaatatggagcacgcaactgctmtatttg-3'), A/V252 R (5'- caatgtcaattccctccgtac-3'), A/V252 F (5'-ccatcgtgcggcccaaccctctagtacggagggaattgacattgtggyttcagctcat-3') and RMLC (5'-gggagggcgtgaatgtaagc-3'). Codon degeneration using XYZ codons (underlined) was explored with amino acid calculator http://guinevere.otago.ac.nz/cgi-bin/aef/AA-Calculator.pl following the protocol previously described (28). The PCR reaction mixtures of the first experiment (**Fig. S6A**) contained: 50 µL final volume, DMSO (3%), dNTPs (1 mM, 0.25 mM each), high-fidelity DNA polymerase iProof (0.02 U/mL), the template *Ev*-PI (10

ng) and the following primers depending on the PCR: PCR1 RMLN (0.5 μM) and S/A61 R (0.5 μM); PCR2 S/A61-L/I79 F (0.5 μM) and A/V252 R (0.5 μM); PCR3 A/V252 F (0.5 μM) and RMLC (0.5 μM). Site-directed mutagenesis (SDM) PCRs to obtain *Ev*-PI-A252L mutant (**Figure S6B**) contained in a 50 μL final volume: DMSO (3%), dNTPs (1 mM, 0.25 mM each), high-fidelity DNA polymerase iProof (0.02 U/mL), the template *Ev*-PI (10 ng) and S/A61 R (0.5 μM)-RMLN (0.5 μM) for fragment 1 (PCR4); and SDM F (5'-ccatcgtgcggcccaaccctctagtacggagggaattgacattgtgttgtcagctcat-3', 0.5 μM)-RMLC (0.5 μM) for fragment 2 (codon with mutation underlined, PCR5). For the second experiment of SDR (**Figure S6C**), the conditions were the following: 50 μL final volume, DMSO (3%), dNTPs (1 mM, 0.25 mM each), high-fidelity DNA polymerase iProof (0.02 U/mL), the template *Ev*-PI-A252L (10 ng) and the following primers depending on the PCR: PCR6 RMLN (0.5 μM) and S/A61 R (0.5 μM); PCR7 S/A61-L/I79 F (0.5 μM) and RMLC (0.5 μM). PCR reactions were carried out on a gradient thermocycler (Mycycler, Bio-Rad, USA), using the following parameters: 98 ºC for 30 s (1 cycle); 98 ºC for 10 s, 48 ºC for 30 s, and 72 ºC for 30 s (28 cycles); and 72 ºC for 10 min (1 cycle). PCR products were loaded onto a preparative agarose gel and purified with the NucleoSpin Gel and PCR Clean-up kit. The recovered DNA fragments were cloned under the control of the GAL1 promoter of the pJRoC30 expression shuttle vector, with use of *Bam*HI and *Xho*I to linearize the plasmid and to remove the parent gene. The linearized vector was loaded onto a preparative agarose gel and purified with the NucleoSpin Gel and PCR Clean-up kit. The corresponding PCR products (200 ng each) were mixed with the linearized plasmid (100 ng) and transformed into *S. cerevisiae* for *in vivo* gene reassembly and cloning by IVOE (35), both the SDR experiments and the SDM experiment. 176 clones were evaluated in each SDR library and 80 in the SDM experiment.

Pab*UPOs expression in *S. cerevisiae

Culture media: Sterile minimal medium for microplate contained 100 mL 6.7% filtered yeast nitrogen base, 100 mL 19.2 g/L filtered yeast synthetic drop-out medium supplement without uracil, 100 mL filtered 20% raffinose, 700 mL *dd*H_2O and 1 mL 25 g/L filtered chloramphenicol. Sterile minimal medium for flasks contained 100 mL 6.7% filtered yeast nitrogen base, 100 mL 19.2 g/L filtered yeast synthetic drop-out medium supplement without uracil, 25 mL filtered 20% glucose, 775 mL *dd*H_2O and 1 mL 25 g/L filtered chloramphenicol. SC drop-out plates contained 100 mL 6.7% filtered yeast nitrogen base, 100 mL 19.2 g/L filtered yeast synthetic drop-out medium supplement without uracil, 20 g autoclaved bacto-agar, 100 mL 20% filtered glucose, 1 mL 25 g/L filtered chloramphenicol and *dd*H_2O to 1,000 mL. Sterile expression medium contained 720 mL autoclaved YP, 67 mL 1 M filtered KH_2PO_4 pH 6.0 buffer, 111 mL 20% filtered galactose, 22 mL filtered $MgSO_4$ 0.1 M, 31.6 mL absolute ethanol (depending on the enzyme), 1 mL 25 g/L filtered chloramphenicol and *dd*H_2O to 1,000 mL. YP medium contained 10 g yeast extract, 20 g peptone and *dd*H_2O to 650 mL. YPD solution contained 10 g yeast extract, 20 g peptone, 100 mL 20% sterile glucose, 1 mL 25 g/L chloramphenicol and *dd*H_2O to 1,000 mL. Luria-Bertani (LB) medium was prepared with 5 g yeast extract, 10 g peptone, 10 g NaCl (5g NaCl for zeocin selection), 100 mg ampicillin or 25 mg zeocin and *dd*H_2O to 1,000 mL. BMMY medium contained 100 mM potassium phosphate buffer pH 6.0, 3.5 g/L yeast nitrogen base without amino acids, 400 µg/L biotin and 0.5% methanol (v:v).

Microtiter plate expression: Individual clones were picked and cultured in sterile 96-well plates containing 50 µL of minimal medium for microplate. In each plate, column 6 was inoculated with PaDa-I and well H1 was not inoculated (culture media control). Plates were sealed to prevent evaporation and incubated at 30 ºC, 225 rpm, and 80% relative humidity in a humidity shaker (Minitron-INFORS; Biogen, Spain). After 48 h, 150 µL of expression medium were added to each well, followed by culture for additional 48 h at 25 ºC. The plates

were centrifuged at 2,000 rpm (at 4 ºC) and finally, 20 µL portions of the supernatants were screened for activity with DMP. The plasmids from positive wells were recovered with Zymoprep yeast plasmid miniprep kit I. Since the product of the Zymoprep was impure and the DNA extracted was very low concentrated, the shuttle vectors were transformed into supercompetent *E. coli* XL2-Blue cells and plated onto LB-ampicillin plates. Single colonies were selected to inoculate 5 mL of LB-ampicillin medium and incubated overnight at 37 ºC and 225 rpm. The plasmids were extracted (NucleoSpin plasmid kit), sent for DNA sequencing (GATC Biotech-Eurofins, Luxembourg) and transformed into *S. cerevisiae* for flask production.

Small-scale flask fermentation: A single colony from the *S. cerevisiae* clone containing the gene of interest was picked from a SC drop-out plate, inoculated in minimal medium for flasks (10 mL) and incubated for 48 h at 30 ºC and 230 RPM. An aliquot of cells was removed and used to inoculate minimal medium (100 mL) in a 500 mL (OD_{600} = 0.25). The cells completed two growth phases (6–8 h) and then expression medium (900 mL) was inoculated with the pre-culture (100 mL) (OD_{600} of 0.1). After incubating for 72 h at 25 ºC and 230 rpm (maximal UPO activity; OD_{600} = 25-30), the cells were recovered by centrifugation at 4,500 rpm (4 ºC) and the supernatant was double-filtered (using both glass membrane and a nitrocellulose membrane of 0.45 µm pore size).

Pab*UPOs expression in *P. pastoris

Cloning, selection and small-scale flask fermentation: The DNA sequences containing Grogu and recombinant *Pab*UPO-II (both preceded by the evolved signal peptide from PaDa-I mutant) were cloned into the expression vector pPICZ-B. The vector pJRoC30-Grogu, resulting from SDR experiments and pJRoC30-*Pab*UPO-II were used to amplify the evolved UPO with the primers psnUPO1DIR2 (5'-ccg**gaattc**ATGAAATATTTTCCCCTGTTCCCAA-3') and PabUPOI R (5'-

gc**tctaga**TCATAGTTGACCGTAGGGGA-3') or psnUPO1DIR2 and PabUPOII R (5'-gc**tctaga**TCAAAGTTGACCGTACGGGA-3'), which included targets for *Eco*RI and *Xba*I restriction enzymes, respectively (in bold; capital letters correspond to each UPO sequence). PCR reactions were performed using a thermocycler (Mycycler, Bio-Rad, USA) in a final volume of 50 µL containing 0.5 µM of each primer, 100 ng template, 1 mM dNTPs (0.25 mM each), DMSO (3%) and high-fidelity DNA polymerase iProof (0.02 U/mL). The PCR conditions were 98 ºC for 30 s (1 cycle); 98 ºC for 10 s, 55 ºC for 27 s, 72 ºC for 30 s (28 cycles); and 72 ºC for 10 min (1 cycle). The pPICZ-B vector and the PCR product were digested with the restriction enzymes *Eco*RI and *Xba*I at 37 ºC for 20 min. The linearized pPICZ-B vector 5' and 3' ends were dephosphorylated using Antarctic phosphatase (1 U per every 200 ng of linearized vector) at 37 ºC for 1 h. The PCR product and the linearized vector were loaded onto a preparative agarose gel, purified using the NucleoSpin Gel and PCR Clean-up kit and ligated with T4 DNA ligase at room temperature for 60 min. After transformation of the pPICZ-B-Grogu and pPICZ-B-*Pab*UPO-II constructs into chemically competent *E. coli* XL2-Blue cells, the plasmid was proliferated, linearized with the restriction enzyme *Pme*I at 37 ºC for 1 h and transformed into electro-competent *P. pastoris* X-33 cells. Electro-competent *P. pastoris* cells were prepared and transformed with the construction as described elsewhere (36) using 1000 ng of linearized vector and 50 µL of competent cells. Transformants were grown on YPD plates (10 g/L yeast extract, 20 g/L peptone, 4 g/L glucose and 15 g/L agar) containing 100, 300 and 500 mg/L zeocin to favor the selection of "high copy number" clones.

Five transformants of each enzyme were inoculated in 3 mL of liquid YPD at 30 ºC and 230 rpm. The culture was refreshed to OD_{600}=0.3 in 10 mL of YPD and grown until it reached an optical density of OD_{600}=1 after 3-4 h and was inoculated in 40 mL of BMMY medium in 500 mL baffled flasks. The cultures were incubated at 30 ºC and they were

supplemented with 500 µl of methanol every 24 hr. After 3 days of methanol addition, the best clone of each enzyme with the highest activity was selected for bioreactor fermentation.

Production in 5-L fed-batch bioreactor

P. pastoris clones containing Grogu and *Pab*UPO-II were cultivated in 5-L glass vessel bioreactor (Biostat® A plus, Sartorius Stedim, Germany) adapted to Pichia Fermentation Process Guidelines of Invitrogen (Version B 053002, Thermo). The basal salts medium (BMG) for the bioreactor with initial volume of 1.7 L contained 26.7 mL/L 85% phosphoric acid, 0.93 g/L $CaSO_4 \cdot 2H_2O$, 14.9 g/L $MgSO_4 \cdot 7H_2O$,18.2 g/L K_2SO_4, 4.13 g/L KOH, 40 g/L glycerol. The PTM_1 Trace salts solution was sterilized by filtration and consists of the following ingredients: 6 g/L $CuSO_4$ $5H_2O$, NaI 0.08 g/L, 3 g/L $MnSO_4$ H_2O, 0.2 g/L Na_2MoO_4, 0.02 g/L H_3BO_3, 0.5 g/L $CoCl_2$, 20 g/L $ZnCl_2$, 65 g/L $FeSO_4$ $7H_2O$, 0.2 Biotin, 5 mL/L sulfuric acid. After autoclaving bioreactor with the media, 4.35 mL/L PTM_1 trace salts and 1 mL Antifoam B (Sigma-Aldrich, Germany) were added. The pH was adjusted to 5.0 with ammonium hydroxide solution (28%) and was kept constant during cultivation. The fermentation process was started by adding 120 mL of *P. pastoris* preculture grown on BMG medium in a 500 mL Erlenmeyer shaking flask at 180 rpm and 30 ºC for 18 h. The glycerol batch was run at 800 rpm and 30 ºC. After the glycerol has been completely consumed, the glycerol fed-batch phase followed with the addition of 50% (*w/v*) glycerol feed, containing 12 mL/L of PTM1 trace salt (dissolved oxygen (DO) concentration should be kept above 20-30%). After completion of the glycerol fed-batch phase, indicated by DO peak after 18 – 24 h, the methanol feed started by adding 3.6 mL/h per liter methanol, containing 12 mL/L PTM1 trace salt. Within the first two to three hours, the addition of methanol was slowly increased so that the culture could adapt and the DO spike stays above 80%. Samples were taken regularly. After methanol is consumed or no increase of enzyme activity can be noticed, the vessel is harvested. Culture of *P. pastoris* cells was clarified by centrifugation at 10,000 x g

for 1 h at 4 ºC. Subsequently, the supernatant was concentrated by ultrafiltration using tangential-flow cassettes (Sartocon Slice Cassette, Hydrosart, cut-off 10 kDa, Sartorius Stedim, Germany).

Purification of Grogu and *Pab*UPO-II

Ammonium sulfate was added slowly to the corresponding ultrafiltrate containing Grogu up to a 40% solution (4 ºC). The resulting suspension was centrifuged at 10,000 g for 1 h at 4 ºC to precipitate non target proteins. Afterwards a hydrophobic interaction chromatography (HIC) with Phenyl Sepharose FF™ (GE Healthcare Europe GmbH, Germany) in a XK 26 x 200 mm column was performed. The bounded proteins were eluted within a linear gradient from 40% to 0% ammonium sulfate in 20 mM BisTris buffer pH 7. The pooled active fraction was applied to anion exchange chromatography on a Mono Q™ 10/100 GL column (GE Healthcare) using 10 mM Na acetate pH 5.5 as mobile phase eluting with a 0.67 M NaCl gradient within 15 column volumes. Finally, this preparation was further isolated via size exclusion chromatography (SEC) on a HiLoad™ Superdex™ 75 pg 26 x 600 mm (GE Healthcare) using 100 mM NaCl in 50 mM Na acetate pH 6.8 as eluent.

The ultrafiltrate of *Pab*UPO-II was applied to Q Sepharose™ FF (GE Healthcare; column: XK 26/20) with 10 mM Na acetate pH 6.0 and a linear gradient 0.67 M NaCl. Eventually a SEC on a HiLoad™ Superdex™ 75 pg 26 x 600 was performed. Homogeneity of the final Grogu and *Pab*UPO-II preparation was proven by SDS-PAGE using precast gels (Invitrogen™ NuPAGE™ Bis-Tris 10 or 12%). The UV-Vis absorption spectra were recorded with Cary 60 UV-Vis Spectrophotometer (Agilent, Germany).

Biochemical characterization

ABTS kinetic constants were estimated in sodium phosphate/citrate buffer (pH 4.0, 100 mM), DMP kinetic constants in phosphate buffer (pH 6.0, 100 mM), and veratryl alcohol, benzyl alcohol, NBD and H_2O_2 in phosphate buffer (pH 7.0, 100 mM). All kinetics except for

H_2O_2 contained a fixed concentration of H_2O_2 (2 mM). H_2O_2 kinetic constants were estimated using veratryl alcohol (8 mM) as reducing substrate. Reactions were performed in triplicate, and substrate oxidations were followed through spectrophotometric changes (ε_{418} $ABTS^{\bullet+}$ = 36,000 M^{-1} cm^{-1}; ε_{469} cerulignone = 27,500 M^{-1} cm^{-1}, ε_{280} benzaldehyde = 1,400 M^{-1} cm^{-1}, ε_{310} veratraldehyde = 9,300 M^{-1} cm^{-1} and ε_{425} 4-nitrocatechol = 9,700 M^{-1} cm^{-1}). To calculate the K_m and k_{cat} values, the average V_{max} was represented against substrate concentration and fitted to a single rectangular hyperbola function with SigmaPlot 10.0, where parameter a was equal to k_{cat} and parameter b was equal to K_m.

pH activity profile with veratryl alcohol was calculated with appropriate dilutions of enzyme samples, prepared in such a way that aliquots of 20 µL gave rise to a linear response in kinetic mode. The optimum pH activity was determined using Britton and Robinson buffer (100 mM) at different pH values (from 2.0 to 9.0), veratryl alcohol (5 mM) and H_2O_2 (2 mM). The activities were measured in triplicate and the relative activity (in percent) is based on the maximum activity at a certain pH for each enzyme.

pH stability profile was calculated with appropriate pure enzyme dilutions incubated at different times over a range of pH values in 20 mM Britton and Robinson buffer (2.0, 3.0, 4.0, 5.0, 6.0, 7.0, 8.0, and 9.0). Samples were removed at different times (0, 15 min, 30 min, 1, 2, 4, 6, and 24 h) and activity was measured in phosphate buffer pH 7.0 (100 mM) with veratryl alcohol (5 mM) and H_2O_2 (2mM). The experiments were performed by triplicate and measured in kinetic mode, and the residual activity was related to the 100% initial activity.

Kinetic thermostability of *Pab*UPOs was estimated by assessing their T_{50} values using 96-well gradient thermocyclers (Mycycler, Bio-Rad, USA). Appropriate UPO dilutions were prepared with the help of the robot in such a way that 20 µL aliquots gave rise to a linear response in the kinetic mode. Then, 50 µL were used for each point in the gradient

scale and a temperature gradient profile ranging from 20 to 80 ºC was established as follows (in ºC): 20.0, 30.0, 31.6, 34.6, 39.5, 45.3, 49.6, 52.8, 55.0, 56.9, 59.9, 64.3, 69.7, 75.0, 78.1 and 80.0. After a 10 min incubation, samples were chilled out on ice for 10 min and further incubated at room temperature for 5 min. Afterwards, 20 µL of samples were assayed in sodium phosphate (pH 6.0, 100 mM), containing H_2O_2 (2 mM) and DMP (2 mM). Reactions were performed in triplicate, and substrate oxidations were followed through spectrophotometric changes. The thermostability values were deduced from the ratio between the residual activities incubated at different temperature points and the initial activity at room temperature.

Purified UPOs (8 µg each) were subjected to two-dimensional electrophoresis gel in order to determine the pI (isoelectric point) at the Protein Chemistry Service from Centro de Investigaciones Biológicas, CIB (CSIC, Spain); and to molecular weight determination by MALDI-TOF at the Proteomics Facility at Centro Nacional de Biotecnología, CNB (CSIC, Spain).

ACKNOWDLEGEMENTS

This work was supported by the Comunidad de Madrid Synergy CAM Project Y2018/BIO-4738-EVOCHIMERA-CM, the Spanish Government Projects BIO2016-79106-R-Lignolution, PID2019-106166RB-100-OXYWAVE and the CSIC Project PIE-201580E042. P. Gomez de Santos is grateful to the Ministry of Science, Innovation and Universities (Spain) for her FPI and POP contracts (BES-2017-080040).

REFERENCES

1. Sigmund M-C, Poelarends GJ. 2020. Current state and future perspectives of engineered and artificial peroxygenases for the oxyfunctionalization of organic molecules. Nat Catal 3:690–702.

2. Hofrichter M, Ullrich R. 2014. Oxidations catalyzed by fungal peroxygenases. Curr Opin Chem Biol 19:116–125.

3. Hofrichter M, Kellner H, Herzog R, Karich A, Liers C, Scheibner K, Kimani VW, Ullrich R. 2020. Fungal peroxygenases: a phylogenetically old superfamily of heme enzymes with promiscuity for oxygen transfer reactions, p. 369–403. *In* Nevalainen, H (ed.), Grand Challenges in Fungal Biotechnology. Springer International Publishing, Cham.

4. Holtmann D, Hollmann F. 2016. The Oxygen Dilemma: A severe challenge for the application of monooxygenases? ChemBioChem 17:1391–1398.

5. Molina-Espeja P, Gomez de Santos P, Alcalde M. 2017. Directed evolution of unspecific peroxygenase, p. 127–143. *In* Alcalde, M (ed.), Directed Enzyme Evolution: Advances and Applications. Springer International Publishing, Cham.

6. Hobisch M, Holtmann D, Gomez de Santos P, Alcalde M, Hollmann F, Kara S. 2020. Recent developments in the use of peroxygenases – Exploring their high potential in selective oxyfunctionalisations. Biotechnol Adv 107615.

7. Molina-Espeja P, Garcia-Ruiz E, Gonzalez-Perez D, Ullrich R, Hofrichter M, Alcalde M. 2014. Directed evolution of unspecific peroxygenase from *Agrocybe aegerita*. Appl Environ Microbiol 80:3496–3507.

8. Molina-Espeja P, Ma S, Mate DM, Ludwig R, Alcalde M. 2015. Tandem-yeast expression system for engineering and producing unspecific peroxygenase. Enzyme Microb Technol 73–74:29–33.

9. Gomez de Santos P, Cañellas M, Tieves F, Younes SHH, Molina-Espeja P, Hofrichter M, Hollmann F, Guallar V, Alcalde M. 2018. Selective synthesis of the human drug metabolite 5′-hydroxypropranolol by an evolved self-sufficient peroxygenase. ACS Catal 8:4789–4799.

10. Gomez de Santos P, Lazaro S, Viña-Gonzalez J, Hoang MD, Sánchez-Moreno I, Glieder A, Hollmann F, Alcalde M. 2020. Evolved peroxygenase–aryl alcohol oxidase fusions for self-sufficient oxyfunctionalization reactions. ACS Catal 13524–13534.

11. Molina-Espeja P, Cañellas M, Plou FJ, Hofrichter M, Lucas F, Guallar V, Alcalde M. 2016. Synthesis of 1-naphthol by a natural peroxygenase engineered by directed evolution. ChemBioChem 17:341–349.

12. Molina-Espeja P, Santos-Moriano P, García-Ruiz E, Ballesteros A, Plou FJ, Alcalde M. 2019. structure-guided immobilization of an evolved unspecific peroxygenase. Int J Mol Sci 20:1627.

13. Mate DM, Palomino MA, Molina-Espeja P, Martin-Diaz J, Alcalde M. 2017. Modification of the peroxygenative:peroxidative activity ratio in the unspecific peroxygenase from *Agrocybe aegerita* by structure-guided evolution. Protein Eng Des Sel 30:191–198.

14. Martin-Diaz J, Paret C, García-Ruiz E, Molina-Espeja P, Alcalde M. 2018. Shuffling the neutral drift of unspecific peroxygenase in *Saccharomyces cerevisiae*. Appl Environ Microbiol 84:e00808-18.

15. Gomez de Santos P, Cervantes FV, Tieves F, Plou FJ, Hollmann F, Alcalde M. 2019. Benchmarking of laboratory evolved unspecific peroxygenases for the synthesis of human drug metabolites. Tetrahedron 75:1827–1831.

16. Martin-Diaz J, Molina-Espeja P, Hofrichter M, Hollmann F, Alcalde M. 2021. Directed evolution of unspecific peroxygenase in organic solvents. Biotechnol Bioeng n/a.

17. Babot ED, del Río JC, Kalum L, Martínez AT, Gutiérrez A. 2013. Oxyfunctionalization of aliphatic compounds by a recombinant peroxygenase from *Coprinopsis cinerea*. Biotechnol Bioeng 110:2323–2332.

18. Püllmann P, Knorrscheidt A, Münch J, Palme PU, Hoehenwarter W, Marillonnet S, Alcalde M, Westermann B, Weissenborn MJ. 2021. A modular two yeast species secretion system for the production and preparative application of unspecific peroxygenases. Commun Biol 4:562.

19. Püllmann P, Weissenborn MJ. 2021. Improving the Heterologous Production of Fungal peroxygenases through an episomal *Pichia pastoris* promoter and signal peptide shuffling system. ACS Synth Biol 10:1360–1372.

20. Knorrscheidt A, Püllmann P, Schell E, Homann D, Freier E, Weissenborn MJ. 2020. Identification of novel unspecific peroxygenase chimeras and unusual YfeX axial heme ligand by a versatile high-throughput GC-MS approach. ChemCatChem 12:4788–4795.

21. Carro J, González-Benjumea A, Fernández-Fueyo E, Aranda C, Guallar V, Gutiérrez A, Martínez AT. 2019. Modulating fatty acid epoxidation vs hydroxylation in a fungal peroxygenase. ACS Catal 9:6234–6242.

22. González-Benjumea A, Carro J, Renau-Mínguez C, Linde D, Fernández-Fueyo E, Gutiérrez A, Martínez AT. 2020. Fatty acid epoxidation by *Collariella virescens* peroxygenase and heme-channel variants. Catal Sci Technol 10:717–725.

23. Linde D, Olmedo A, González-Benjumea A, Estévez M, Renau-Mínguez C, Carro J, Fernández-Fueyo E, Gutiérrez A, Martínez AT. 2020. Two new unspecific peroxygenases from heterologous expression of fungal genes in *Escherichia coli*. Appl Environ Microbiol 86:e02899-19.

24. Melzer A, Kimani VW, Ullrich R. 2018. *Psathyrella aberdarensis*, a new species of *Psathyrella* (Agaricales) from a Kenyan National Park. Austrian J Mycol 27:23–30.

25. Wächter D, Melzer A. 2020. Proposal for a subdivision of the family Psathyrellaceae

based on a taxon-rich phylogenetic analysis with iterative multigene guide tree. Mycol Prog 19:1151–1265.

26. Kimani VW. 2019. New Secretory Peroxidases and Peroxygenases from Saprotrophic Fungi of Kenyan Forests. Ph.D. Thesis. TU Dresden-IHI Zittau. Germany.

27. Ramirez-Escudero M, Molina-Espeja P, Gomez de Santos P, Hofrichter M, Sanz-Aparicio J, Alcalde M. 2018. Structural insights into the substrate promiscuity of a laboratory-evolved peroxygenase. ACS Chem Biol 13:3259–3268.

28. Viña-Gonzalez J, Alcalde M. 2020. Chapter One - In vivo site-directed recombination (SDR): An efficient tool to reveal beneficial epistasis, p. 1–13. *In* Tawfik, DSBT-M in E (ed.), Enzyme Engineering and Evolution: General Methods. Academic Press.

29. Aranda C, Carro J, González-Benjumea A, Babot ED, Olmedo A, Linde D, Martínez AT, Gutiérrez A. 2021. Advances in enzymatic oxyfunctionalization of aliphatic compounds. Biotechnol Adv 107703.

30. Gröbe G, Ullrich R, Pecyna MJ, Kapturska D, Friedrich S, Hofrichter M, Scheibner K. 2011. High-yield production of aromatic peroxygenase by the agaric fungus *Marasmius rotula*. AMB Express 1:31.

31. Alcalde M. 2017. When directed evolution met ancestral enzyme resurrection. Microb Biotechnol 10:22–24.

32. Spence MA, Kaczmarski JA, Saunders JW, Jackson CJ. 2021. Ancestral sequence reconstruction for protein engineers. Curr Opin Struct Biol 69:131–141.

33. Piontek K, Strittmatter E, Ullrich R, Gröbe G, Pecyna MJ, Kluge M, Scheibner K, Hofrichter M, Plattner DA. 2013. Structural basis of substrate conversion in a new aromatic peroxygenase: Cytochrome P450 functionality with benefits. J Biol Chem

288:34767–34776.

34. Ullrich R, Nüske J, Scheibner K, Spantzel J, Hofrichter M. 2004. Novel Haloperoxidase from the Agaric Basidiomycete *Agrocybe aegerita* Oxidizes Aryl Alcohols and Aldehydes. Appl Environ Microbiol 70:4575–4581.

35. Alcalde M. 2010. Mutagenesis protocols in *Saccharomyces cerevisiae* by in vivo overlap extension, p. 3–14. *In* Braman, J (ed.), In Vitro Mutagenesis Protocols: Third Edition. Humana Press, Totowa, NJ.

36. Lin-Cereghino J, Wong WW, Xiong S, Giang W, Luong LT, Vu J, Johnson SD, Lin-Cereghino GP. 2005. Condensed protocol for competent cell preparation and transformation of the methylotrophic yeast *Pichia pastoris*. Biotechniques 38:44–48.

Table 1. Biochemical features of recombinant *Pab*UPOs expressed in *P. pastoris*.

Biochemical and Spectroscopy features	Grogu	*Pab*UPO-II
MW (Da)[1]	47,000	45,000
MW (Da)[2]	42,491	41,247
MW (Da)[3]	36,500	37,700
Glycosylation degree (%)	14	9
Thermal stability, T_{50} (ºC)	56	61
pI	5.3	5.1
Specific activity (U/mg)[4]	82.9	205.9
Production levels (mg/L) in bioreactor	240	290
Optimum pH for peroxygenase activity[5]	6.0	5.0
pH range for peroxygenase activity[6]	3-9	4-7
R_Z (A_{410}/A_{280})	2.63	1.71
Soret region (nm)	417	420
CT1 (nm)	567	570
CT2 (nm)	538	537

[1]Estimated by SDS-PAGE; [2]Estimated by MALDI-TOF mass spectrometry; [3]estimated from amino acid composition (ProtParam); [4,6]measured with veratryl alcohol; [5]pH range in which UPO variant keeps over 40% of relative activity measured with veratryl alcohol. See Supplementary Figures S3, S4, S5.

Table 2. Steady kinetic parameters of wild type and recombinant *Pab*UPOs.

Variant	Kinetic Constant	ABTS	DMP	NBD	Veratryl alcohol	Benzyl alcohol	H_2O_2
Grogu	K_m (μM)	201 ± 10	357 ± 44	434 ± 53	1,277 ± 288	2,259 ± 441	107 ± 12
	k_{cat} (s^{-1})	117 ± 2	27 ± 1	29 ± 1	28 ± 3	254 ± 32	33 ± 1
	k_{cat}/K_m (mM^{-1} s^{-1})	582	76	67	22	112	308
*Pab*UPO-II	K_m (μM)	243 ± 5	397 ± 89	354 ± 48	4,006 ± 216	6,675 ± 348	411 ± 60
	k_{cat} (s^{-1})	97 ± 1	87 ± 7	22 ± 1	106 ± 4	214 ± 7	114 ± 7
	k_{cat}/K_m (mM^{-1} s^{-1})	679	219	62	26	32	277
Wild type *Pab*UPO-I*	K_m (μM)	105	656	---	856	---	---
	k_{cat} (s^{-1})	20	23	---	20	---	---
	k_{cat}/K_m (mM^{-1} s^{-1})	190	35	---	23	---	---
Wild type *Pab*UPO-II*	K_m (μM)	128	143	---	1,291	---	---
	k_{cat} (s^{-1})	85	50	---	104	---	---
	k_{cat}/K_m (mM^{-1} s^{-1})	664	350	---	80	---	---

*Values from Ref (26).

Figure 1

Figure 1. Sequence alignment of mature *Pab*UPOs and the PaDa-I enzyme. The mutations acquired during the directed evolution campaign of PaDa-I are highlighted in grey and their corresponding positions in the *Pab*UPOs are in square boxes (created by Clustal Omega - https://www.ebi.ac.uk/Tools/msa/clustalo/).

Figure 2

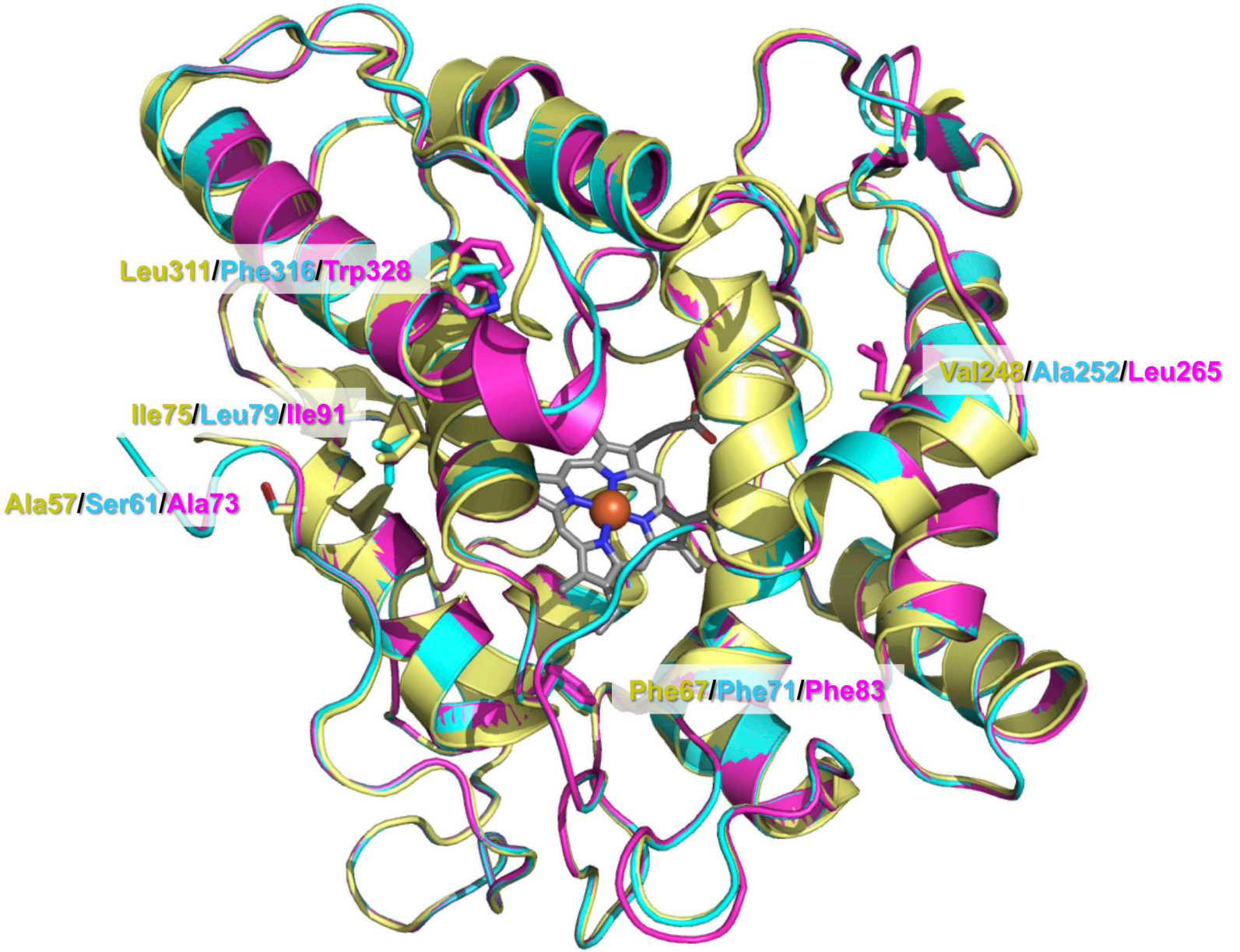

Figure 2. Homology models of *Pab*UPO-I (blue cyan) and *Pab*UPO-II (magenta) compared to the PaDa-I crystal structure (yellow). The models were generated using SWISS-MODEL (https://swissmodel.expasy.org/) and they are based on the crystal structure of the PaDa-I mutant (pdb number 6EKZ) visualized with PyMOL (https://pymol.org). The five secretion mutations in PaDa-I are depicted as bars and sticks.

Figure 3

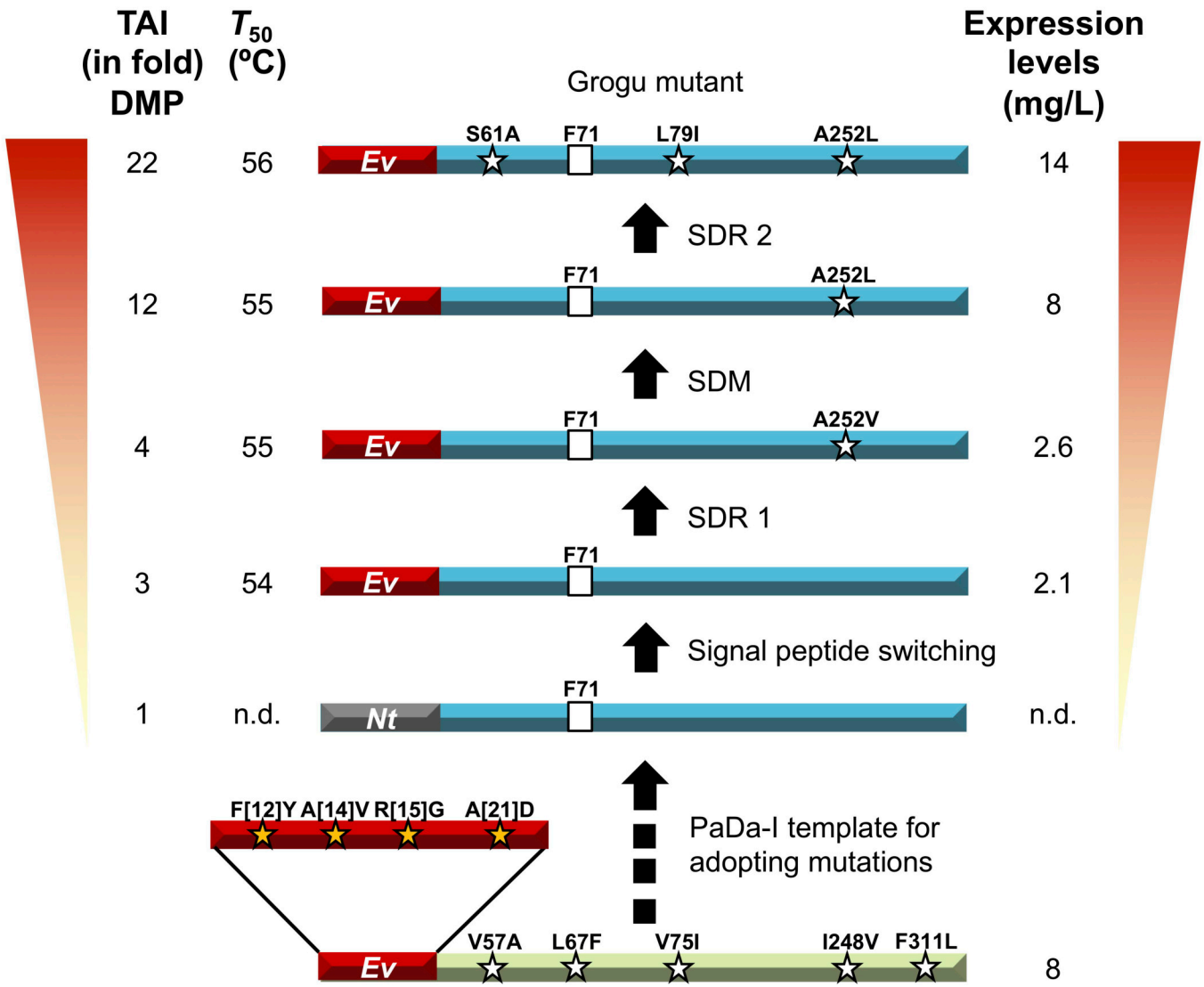

Figure 3. Engineering of the Grogu mutant. Stronger expression (2.1 mg/L) was achieved by replacing *Nt* with *Ev*. The *Ev*-PI SDR mutant library (SDR 1) included the S61A-L79I-A252V mutations and their corresponding reversions. The best selected mutant (2.6 mg/L) only incorporated the A252V mutation. Given that *Pab*UPO-II has a Leu residue at this position, we introduced the A252L substitution by site directed mutagenesis (SDM), which increased secretion to 8 mg/L. Finally, we created a new SDR mutant library (SDR 2) for the mutations S61A-L79I-A252L and their reversions, yielding the triple (Grogu variant) expressed at 14 mg/L. The stars indicate mutations and the squares (F71) represents the exact match between wildtype *Pab*UPO-I and PaDa-I: TAI, total activity improvement over *Nt*-EPI measured with DMP as a substrate.

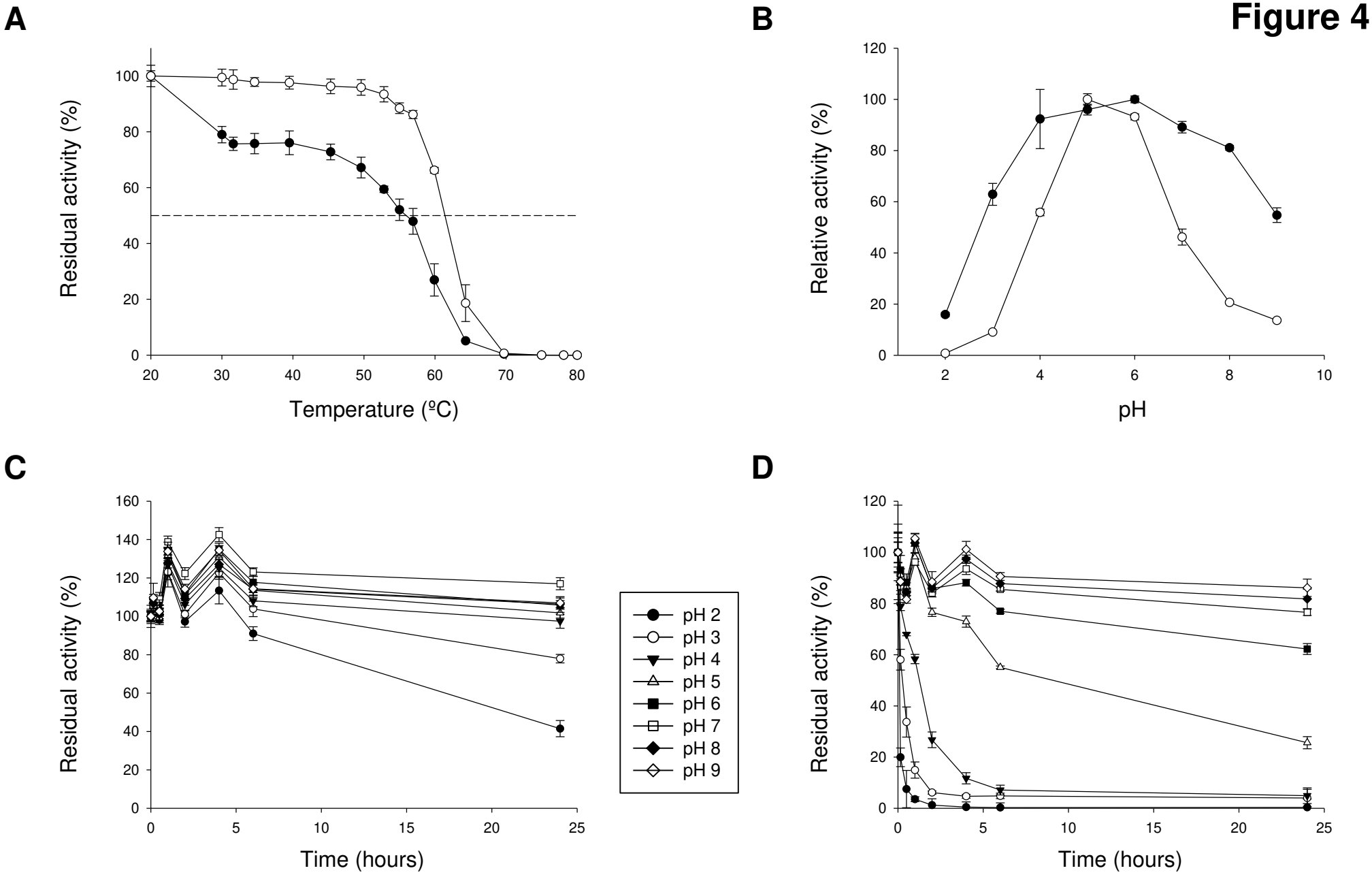

Figure 4. Biochemical characterization. (**A**) Kinetic thermostability (T_{50}) and (**B**) pH activity profile measured with 5 mM veratryl alcohol and 2 mM H_2O_2 in 100 mM Britton and Robinson buffer at different pHs from 2.0 to 9.0: black circles, Grogu mutant; white circles *Pab*UPO-II. (**C**) and (**D**) pH stability profiles for Grogu and *Pab*UPO-II, respectively. Appropriate enzyme dilutions were incubated at different times over a range of pH values in 20 mM Britton and Robinson buffer. Aliquots were removed at different times to measure activity with 5 mM veratryl alcohol and 2 mM H_2O_2 in 100 mM phosphate buffer pH 7.0 at room temperature. Each point represents the mean and standard deviation of 3 independent experiments.

Figure 5

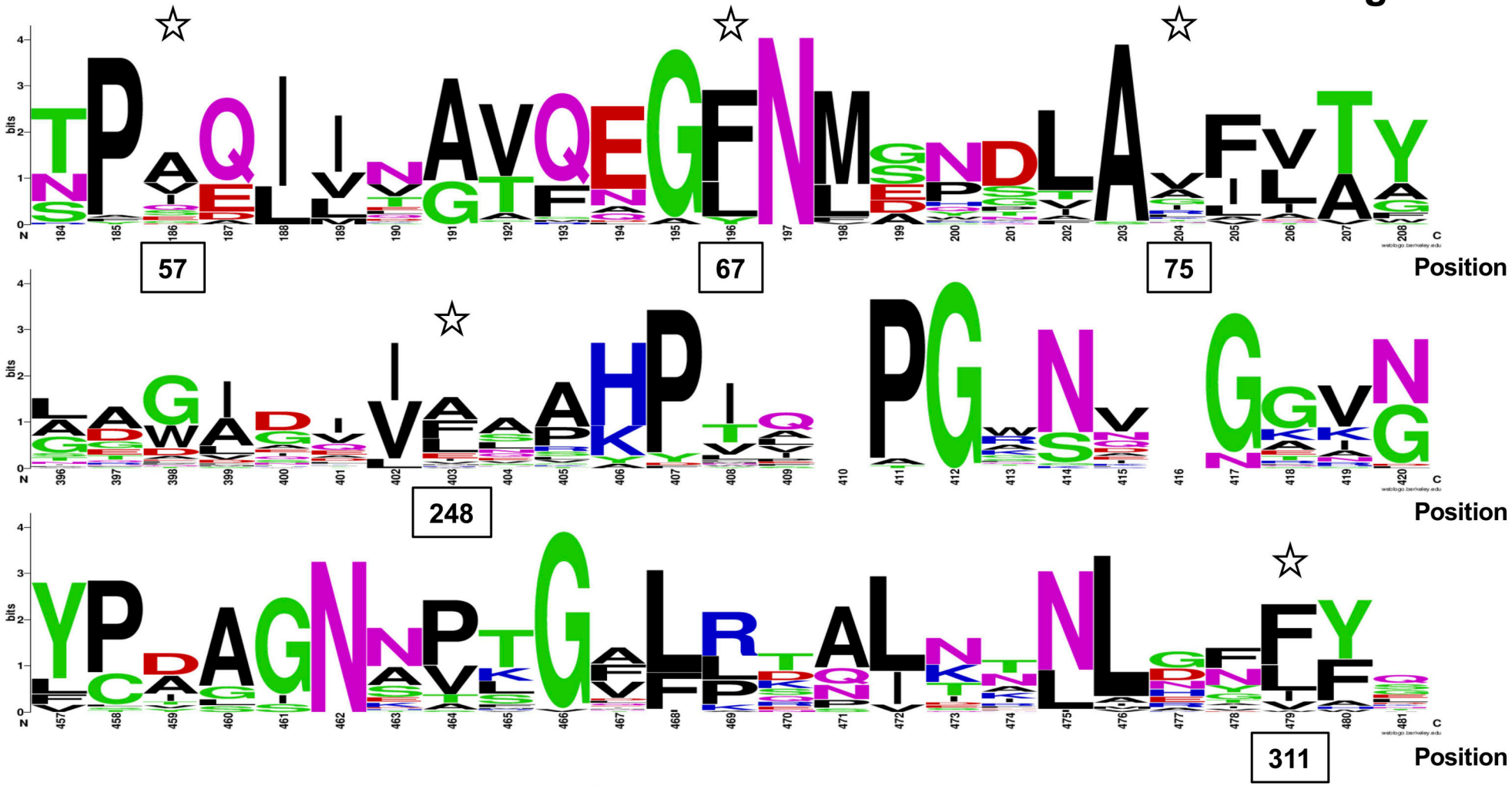

Figure 5. Sequence logo of the regions harboring functional expression mutations calculated with the 50 UPO sequences in GenBank (http://www.ncbi.nlm.nih.gov/GenBank/). Figure created with https://weblogo.berkeley.edu/logo.cgi.

Figure 6

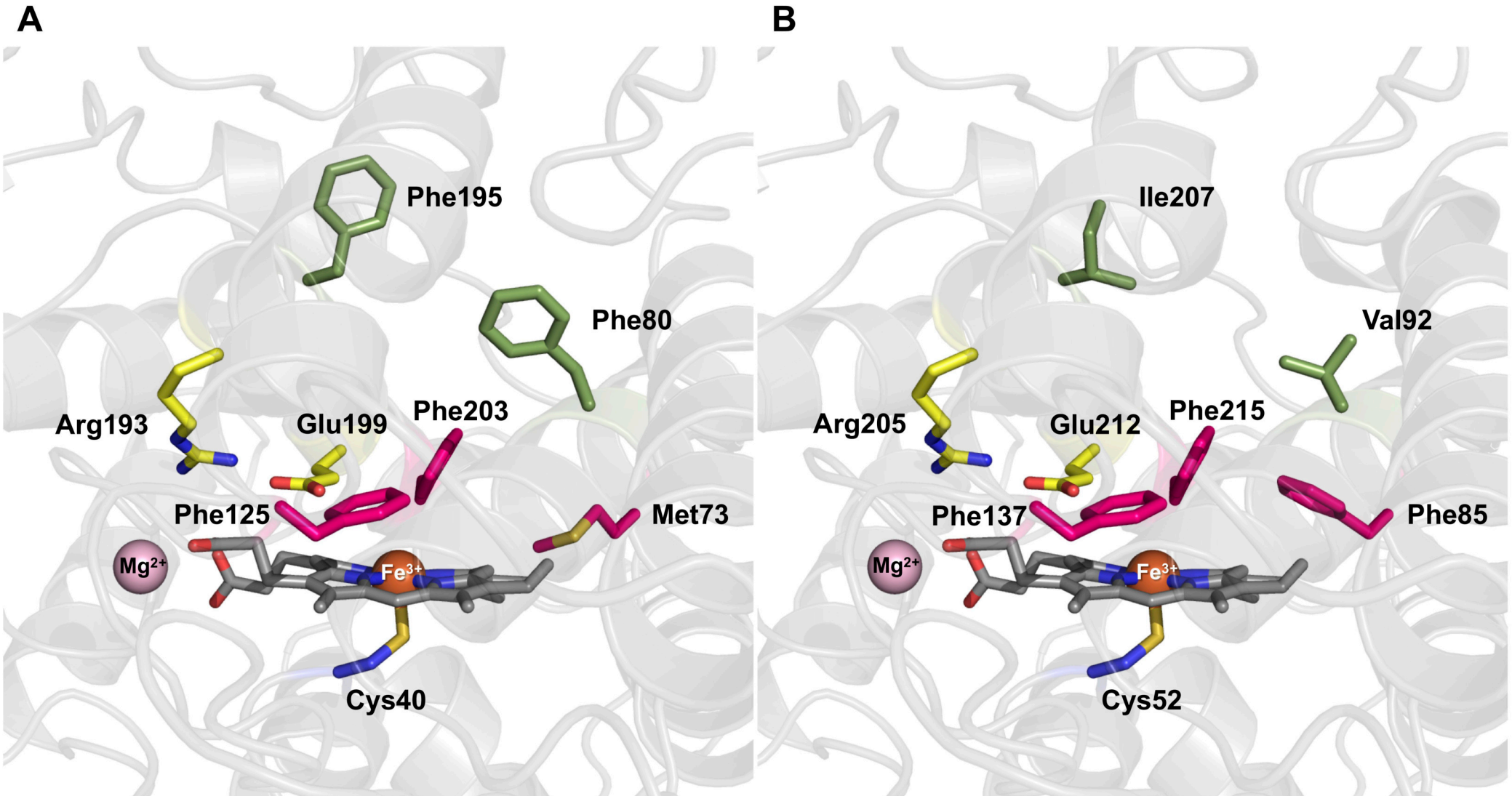

Figure 6. Details of the active site of the (**A**) Grogu mutant and (**B**) *Pab*UPO-II. Acid base pairs are depicted in yellow, proximal ligand (5th) Cys in blue, and the amino acids involved in orienting the substrate for catalysis in pink. The amino acids at the entrance of both channels are colored in green. Both models were generated by SWISS-MODEL (https://swissmodel.expasy.org/) using the crystal structure of the PaDa-I mutant as a template (pdb number 6EKZ), visualized with PyMOL (https://pymol.org).